

## Numerical modeling of translational dynamics for shallow landslides based on flume tests – special case of spherical-cap-shaped slope sections

J. Kanule & W. Ng'etich

To cite this article: J. Kanule & W. Ng'etich (2020) Numerical modeling of translational dynamics for shallow landslides based on flume tests – special case of spherical-cap-shaped slope sections, *Geology, Ecology, and Landscapes*, 4:2, 151-158, DOI: [10.1080/24749508.2019.1608408](https://doi.org/10.1080/24749508.2019.1608408)

To link to this article: <https://doi.org/10.1080/24749508.2019.1608408>



© 2019 The Author(s). Published by Informa UK Limited, trading as Taylor & Francis Group.



Published online: 25 Apr 2019.



[Submit your article to this journal](#)



Article views: 225



[View related articles](#)





[View Crossmark data](#)



Citing articles: 1 [View citing articles](#)

## Numerical modeling of translational dynamics for shallow landslides based on flume tests – special case of spherical-cap-shaped slope sections

J. Kanule <sup>a</sup> and W. Ng'etich <sup>b</sup>

<sup>a</sup>Department of Physics, University of Eldoret, Eldoret, Kenya; <sup>b</sup>Department of Soil Science, University of Eldoret, Eldoret, Kenya

### ABSTRACT

Slope failures can endanger human life and cause infrastructural destruction and socio-economic loss. Geoscientists have strived to develop constitutive models and real-time slope monitoring models and systems to abate these processes. Most research studies have proposed models which describe the dynamics of wedge-shaped soil masses which do not mimic real field conditions. In this study, failure dynamics of spherical-cap-shaped soil masses on an inclined slope section undergoing purely translational displacement are described using empirical models derived from inertial forces in action for varying hydrological conditions. Validation of model results was done through experimental tests carried out on a laboratory flume. Empirical models representing rainfall intensity, soil water content, pore-water pressure, factor of safety, and displacement were derived. More pertinently, the empirical model for the factor of safety is derived considering the moist unit weight of the soil as opposed to earlier models which focused on saturated conditions only. Model and experimental results indicate close concurrence, especially for the factor of safety with root mean square error of 0.0385 and  $r^2$  of 0.6381. Since the models are physics based, they can be applied on a variety of rainfall-induced shallow landslides on relatively steep slopes.

### ARTICLE HISTORY

Received 12 September 2018  
Accepted 13 April 2019

### KEYWORDS

Translational failure;  
numerical model; shallow  
landslides

## 1 Introduction

Many incidences of soil mass movements including but not limited to landslides or mudslides have been reported lately in many parts of Kenya (especially in the Rift valley, central and western highlands), claiming a sizeable number of populace and enormous destruction to infrastructure leading to general socio-economic meltdown. Sloping regions are considered as environmentally sensitive areas where many land development activities for agricultural production, agro-tourism, property development, and road construction projects are ongoing with high prospects of other infrastructural expansions. While the impacts of soil mass movement incidences have had negative insinuations on the socioeconomic profile of the regional general development, there exist a number of gaps in terms of the theoretical formulation, monitoring, and mitigative measures.

For any form of soil mass wasting to occur, certain precursory factors set the stage for triggering events that initiate failure (Rybar, Stemberk, & Wagner, 2002). The most common triggers of landslides are precipitation, seismicity, and human activities (Petley, 2009). According to earlier studies, water reduces shear strength of a soil mass either by accelerating the process of crack formation and development or lubricating the soil grains by filling the pore spaces (Anderson & Anderson, 2010; Kilburn & Petley,

2003). Fang, Cui, Pei, and Zhou (2012) reported that shallow landslides occur as a result of sudden loss of shear resistance when high pore-water pressures develop leading to liquefaction due to cyclic loading. While high-intensity, short-duration rainfall events are known to trigger soil mass movements, even long-duration, low-intensity rainfall and rapid snow or ice melt also activate landslides (Guzzetti, Ardizzone, Cardinali, Rossi, & Valigi, 2009). Earthquakes of magnitude greater than  $M = 4.0$  may generate strong ground shaking movements which rapidly reduce the frictional strength and/or increase shear stress of hillslope material through rock mass shattering or liquefaction, thereby triggering landslides (Meunier, Hovius, & Haines, 2008).

Several slope dynamic models including Janbu, Mertens, and Bishops have been utilized in many cases to provide an analytical equation relating certain parameters of the physical system to its temporal behavior in space. All these models highlight the factor of safety as an indicator of the health status of the slope for a given set of conditions (Najjar, Ali, & Basheer, 1999). Incidentally, there exist some cases where these models are inapplicable because of the inherent nonlinearity of the system, lack of experimental information, experimental inaccuracy, and deviations from the ideal conditions (Shahin, Jaksa, & Maier, 2001). In addition, since many factors are used as inputs in modeling slope

stability, most of these models cannot replicate physical occurrences in nature, especially when describing vital factors such as slope geometry and soil properties affecting the stability of slopes (Jia, Zhan, Chen, & Fredlund, 2009).

Soil mass movement processes are studied with a view to develop physical models based on geomorphological factors (slope gradient, aspect, and relative relief), soil characteristics (depth, structure, permeability, and porosity), and hydrological factors, which can be employed in the characterization of a wide range of slope sections. In this study, empirical physics-based models are derived from first principles based on inertial forces that build up when a soil mass is inclined at an angle under modest wetting conditions. The objective of the study is to investigate translational motion beginning from inertial forces acting on a soil mass, to the buildup of pore pressures and shear stresses to the effect of these forces on the factor of safety and by extension the displacement downslope.

## 2 Materials and methods

### 2.1 Model formulation

A numerical model is proposed that describes the dynamics of a soil mass inclined at an angle,  $\alpha$ . In this study, we consider the simplified case of a nearly concave-shaped slope section that resembles a spherical cap of relatively small height inclined at an angle of  $\alpha$  to the horizontal and of approximately infinite lateral extent as depicted in [Figure 1](#). The soil mass is considered as a homogeneous rigid-perfectly plastic material which undergoes shear failure when driving and frictional forces are not balanced. The volume in consideration is illustrated by the portion *abcd* which is approximated to a spherical cap of height  $H\cos\alpha$  and base length  $L$ . From the definition

of the volume of a spherical cap, we derive the weight of a dry soil skeleton of nearly the same shape as

$$W_d = \frac{\pi\gamma_d H \cos\alpha}{6} \left( \frac{3L^2}{4} + H^2 \cos^2\alpha \right) \quad (1)$$

where  $\gamma_d$  is the dry unit weight of the soil defined by

$$\gamma_d = \frac{G\gamma_w}{1+e} \quad (2)$$

with  $G$ , the specific gravity of soil; and  $e$ , the void ratio.

For a soil mass under wetting conditions usually through a rainfall simulator or irrigation event (introduction of water into the soil crystal matrix), the new weight of the saturated soil segment assuming there is negligible run-off is

$$W_s = \frac{\pi\gamma_e H \cos\alpha}{6} \left( \frac{3L^2}{4} + H^2 \cos^2\alpha \right) \quad (3)$$

where  $\gamma_e$  is the effective unit weight of the soil defined by De Vleeschauer and De Smedt (2002) as

$$\gamma_e = \frac{q \cos\alpha}{H} + (1-m)\gamma_d + m\gamma_s \quad (4)$$

for which  $q$  is the additional weight on the soil surface by vegetation or structures. The factor  $m$  in Equation (5) is the wetness index defined by Ray, Jacobs, and de Alba (2010) as

$$m = \frac{h + (H-h)S}{H} = \frac{h + (H-h)\left(\frac{\theta}{n}\right)}{H} \quad (5)$$

where  $h$  is the saturated thickness of the soil above the failure plane and  $S = \theta/n$  is the degree of saturation;  $n$  is the soil porosity and  $\theta$  is the volumetric moisture content derived from the modified soil-water characteristic curve proposed by Fredlund and Xing (1994) as

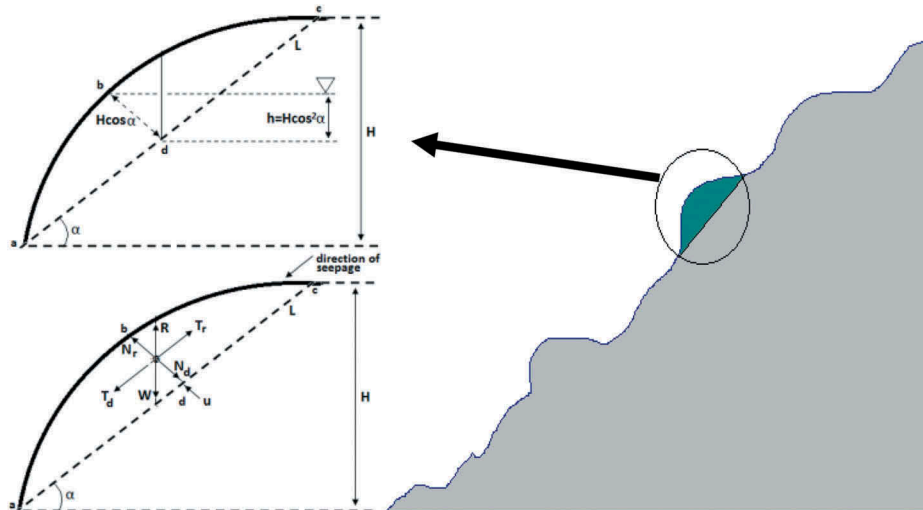


**Figure 1.** Schematic representation of a spherical-cap-shaped slope section (shaded) and the inertial forces acting on it.

$$\theta = \left[ 1 - \frac{\ln\left(1 + \frac{\psi}{\psi_r}\right)}{\ln\left(1 + \frac{10^6}{\psi_r}\right)} \right] \left[ \frac{\theta_s}{\left[\left[\ln\left(e_n + \frac{\psi}{\beta}\right)^p\right]\right]^q} \right] \quad (6)$$

where  $\theta_s$  is the saturated volumetric water content,  $\psi$  is the soil suction,  $\psi_r$  is the residual soil suction,  $e_n$  is a natural number, while  $\beta$ ,  $p$ , and  $q$  are curve fitting parameters with  $\beta$  carrying the units of pressure.

For the model proposed by De Vleeschauwer and De Smedt (2002) (Equation 4), the effective unit weight of the soil is valid with its assumption that water pressures in the wet pores are transmitted to the failure plane through the interconnected wet soil pores. In contrast, we propose that for more precise results, the unsaturated zone soil moisture content must be accounted for in the computation of the wetness index and the effective unit weight as opposed to earlier studies where the effective unit weight of the soil was considered either for purely saturated conditions or on purely dry soil skeleton. Based on earlier studies by Sidle and Ochiai (2006), we propose substitution of the dry unit weight with the moist unit weight ( $\gamma_m$ ) in Equation (4) resulting in

$$\gamma_{em} = \frac{q \cos \alpha}{H} + (1 - m)\gamma_m + m\gamma_s \quad (7)$$

where

$$\gamma_m = G\gamma_w(1 - n)(1 + \theta) \quad (8)$$

is the moist unit weight.

The total weight of moist unsaturated soil ( $W_{\text{moist}}$ ) will now be obtained by utilizing Equation (7) as

$$W_{\text{moist}} = \frac{\pi\gamma_{em}H \cos \alpha}{6} \left( \frac{3L^2}{4} + H^2 \cos^2 \alpha \right) \quad (9)$$

Consequently, by definition, we derive the effective normal and shear stresses for moist soil mass, respectively (considering the base area =  $\pi L^2/4$ ) as

$$\sigma_n = \frac{2\gamma_{em}H \cos^2 \alpha}{3} \left( \frac{3}{4} + \frac{H^2}{L^2} \cos^2 \alpha \right) \quad (10)$$

and

$$\tau_d = \frac{2\gamma_{em}H \cos \alpha \sin \alpha}{3} \left( \frac{3}{4} + \frac{H^2}{L^2} \cos^2 \alpha \right) \quad (11)$$

The proposed empirical model for precipitation for a given period of time is derived from an odd Fourier Series expression as

$$Rn(t) = k \sum_{\eta=1}^{\infty} \frac{\sin(2\eta - 1)t}{(2\eta - 1)} \quad (12)$$

where  $k$  and  $\eta$  are curve fitting parameters.

The pore-water pressure in the soil mass for a piezometer placed at point  $h$  is given by

$$u = \gamma_w h = \gamma_w H \cos^2 \alpha \quad (13)$$

while the soil cohesion which is a function of the water content and soil lithology has been empirically modeled as

$$c' = a\theta^{-1}e^{-\frac{b}{\theta}} \quad (14)$$

where  $a$  is a curve fitting parameter, while  $b$  is a factor related to the observable soil suction for water.

Assuming that there is minimal seepage through the soil mass in consideration and that the groundwater level in this segment is parallel to the incline plane, i.e., coincides with the ground surface adjacent to it, then the shear stress of the soil with effective cohesion  $c'$  and effective angle of shear resistance  $\phi'$  is given by (Bishop, 1967):

$$\tau_r = c' + (\sigma - u) \tan \phi'$$

or

$$\tau_r = c' + \left[ \frac{2\gamma_{em}H \cos^2 \alpha}{3} \left( \frac{3}{4} + \frac{H^2}{L^2} \cos^2 \alpha \right) - \gamma_w H \cos^2 \alpha \right] \tan \phi' \quad (15)$$

Assuming that slope stability is characterized by the Mohr-Coulomb failure criterion and that there are no external loads, the factor of safety will then be computed by

$$FS = \frac{2c' \csc 2\alpha}{\Theta \gamma_{em} H} + \left( 1 - \frac{1}{\Theta} \frac{\gamma_w}{\gamma_{em}} \right) \frac{\tan \phi'}{\tan \alpha} \quad (16)$$

where  $\Theta = \frac{2}{3} \left( \frac{3}{4} + \frac{H^2}{L^2} \cos^2 \alpha \right)$ .

The acceleration of the soil mass downslope has been modeled by the relation

$$a = g\Phi(1 - FS)[\sin \alpha - \cos \alpha \tan \phi] \quad (17)$$

where  $\Phi$  is a curve fitting parameter. This, therefore, leads to the derivation of the equations of motion for velocity and displacement components, respectively, as

$$v = \{2gH\Phi(1 - FS)(\sin \alpha - \cos \alpha \tan \phi)\}^{\frac{1}{2}} \quad (18)$$

$$S = \frac{v^2}{2a} \quad (19)$$

## 2.2 Experimental setup

The experimental tests were conducted in the Soil Science Lab at the University of Eldoret. Soil samples used in the experiments were taken from Sergoit swamp with predominantly ferrallic cambisol soils. A solar-powered monitoring (SPM) system was fabricated comprising a model flume installed with both electronic and optical displacement sensors connected to a data acquisition panel. The dimensions of the model flume were 1.6 m long, 0.6 m width, and 0.5 m high (Figure 2). The model flume was made up of a metallic framework with wooden sheets on the sides.



**Figure 2.** SPM system setup.

A rainfall simulator consisting of a water source, nozzle array, and a flow rate controller was used. It was mounted on the system in such a way that the flow rate could be controlled remotely via an electronic switch. Monitoring of the incident rainfall was realized via a Steven's rain gauge which was wirelessly connected to a Steven's Vantage Console for onward transmission of data to a remote computer. Pore-water pressure in the soil mass was measured by vibrating wire piezometer connected to a 4–20-mA data logger. Soil moisture content and displacement were monitored using Arduino-based resistivity and ultrasonic transducers, respectively. Arduino-based sensors were connected to a microprocessor for interface with a PC. A flowchart of data from the array of transducers to the data loggers connected to the remote server is shown in [figure 4](#).

Two experiments were carried out with a rainfall simulator, while one control system was set up with no rainfall applied to it. For each soil sample collected, approximately 80% of it ( $\approx 120$  kg) was placed in the model flume to form a single flat layer and then the remaining 30 kg was poured at the center to form the spherical-cap-shaped mass. No compaction of the soil was conducted. One side of the flume was then tilted at an angle of  $58^\circ$  to the horizontal using a high-lift jack. Failure of the soil mass was facilitated by the use of an artificial rainfall from the simulator. The spherical-cap-shaped model of the slope was chosen from the fact that, for a given slope of relatively high gradient with negligible vegetation cover, due to uneven erosion incidences, moderate bump-shaped soil masses are left behind which resemble spherical caps of finite length along the incline plane.

### 2.3 Data analysis

Statistical error estimates such as root mean square error (RMSE), coefficient of correlation, and coefficient of determination ( $r^2$ ) were employed to analyze the

performance of the models against laboratory results (Nahm, 2016). The RMSE is the measure of the difference between values predicted by a model and the actual experimental values defined mathematically as

$$RMSE = \sqrt{\frac{\sum_{i=1}^j (X_{obs,i} - X_{model,i})^2}{j}} \quad (20)$$

where  $X_{obs}$  and  $X_{model}$  are observed and modeled values at time/place  $i$ , respectively, while  $j$  is the number of data points.

On the other hand, the correlation coefficient indicates the strength and direction of a linear relationship between model output and experimental values. For a series with  $i$  observations and  $j$  model values, the correlation coefficient is used to estimate the correlation between model and observations as

$$r = \frac{\sum_{i=1}^j (x_{obs,i} - \bar{x}_{obs}) \cdot (x_{model,i} - \bar{x}_{model})}{\sqrt{\sum_{i=1}^j (x_{obs,i} - \bar{x}_{obs})^2 \cdot \sum_{i=1}^j (x_{model,i} - \bar{x}_{model})^2}} \quad (21)$$

If the correlation is +1, it indicates the case of a perfect increasing linear relationship and  $-1$  if it is a decreasing linear relationship. Values in between +1 and  $-1$  indicate the degree of linear relationship between two sets of observations. A correlation coefficient of 0 implies there is no linear relationship between the variables. The square of the correlation coefficient ( $r^2$ ) indicates how much of the variance between the two variables is described by the linear fit.

## 4 Results and discussion

The use of computational methods in determining soil mass dynamics makes it possible to evaluate, with a sufficient degree of precision and in a simple manner, the characteristics of a given slope under conditions of intense but periodic rainfall or irrigation events modeled from simple physics-based equations.



Data from numerical results arising from the derived model are then compared with experimental data obtained from the model flume for purposes of validation. Although the validation samples were independent of *in-situ* field conditions because they were disturbed in one way or the other during sample collection, the geology and soil properties are kept unchanged. Three samples were tested, one of which was a control experiment. The results of each parameter measured were recorded and an average computed that was then used in the model for comparison.

Using a rainfall simulator, incident rainfall event was maintained at 45 mm for 45 min and then stopped for all the experiments. This condition was adhered to in order to study the effects of pore-water pressures on the soil mass and its dependence on the soil moisture content. Computational results from the proposed model (Equation 11) for a single rainfall event as a function of time were compared to experimental data as illustrated in Figure 3(a). From the plot, the RMSE and Pearson correlation coefficient of 3.9385 and 0.9819, respectively, were obtained between model results and experimental laboratory data. This implies that the accuracy of the proposed model is relatively high.

In this experiment, it is assumed that infiltrating water serves to increase the weight of the soil mass (and by extension the normal stress) and alter the cohesion depending on the degree of saturation. The variation of the moisture content over time for both model and experimental data is illustrated in Figure 3(b). The amount of moisture content in the soil mass is a function of the specific moisture capacity, specific storage (computed as the inverse of the soil skeleton bulk modulus), pore-water pressure (negative in unsaturated zone), time elapsed, relative permeability, dynamic viscosity of water, and vertical elevation coordinate (van Genuchten, 1980). Volumetric soil moisture content is found to rise from a modest value of 20% to nearly saturation, i.e., about 93%, when the soil mass begins to move downslope. This is observed from the development of numerous cracks which begin to coalesce into bigger ones as moisture content increases steadily. Because of the high plastic strength of the type of soil sampled, a very high degree of saturation was required to reach failure. Additionally, during the experiment, the rainfall simulator was programmed in such a way that when pore-water pressures began to rise, it could be stopped automatically. While the model assumes water content steadily drops after the rainfall event, experimental results deviate slightly showing a nearly exponential decrease, and this is attributed to the specific storage factor for the specific soil mass. Performance comparison of the numerical model to experimental data yielded an RMSE and  $r^2$  of 0.0108 and 0.9291, respectively.

As soil moisture content rises as a result of infiltration, the negative pore-pressures will remain almost constant in the initial stages because not all pore spaces are filled. But after some time (for our case 30 min), there is an exponential rise in the pore-pressure towards the positive phase as saturation conditions approach (Figure 3(c)). Computational results from the model agree well with the experimental data except that after failure, the model envisages a faster drop in pore-pressures, but in the experiment, they remain almost constant for some time since the soil mass must undergo a drying process. It is also observed that the pore-water pressures in the soil mass continue to rise even when the rainfall event has been halted, indicating their strong dependence on infiltration rate rather than rainfall intensity directly. This means that pore-pressures will, therefore, vary according to the moisture content present in the soil at any given time regardless of the source of water whether irrigation event or rainfall. Numerical model results as compared to experimental data produced RMSE and correlation coefficient of 0.5473 and 0.9261, respectively, which indicates a close concurrence.

Addition of water into a soil mass on a slope through rainfall infiltration or irrigation event serves to increase the weight of the sliding plane and lubricating the soil particles, thereby increasing the driving forces downslope and/or significantly reducing the shear resistive forces consequently leading to a drop in the factor of safety. The value of the factor of safety indicates the health status of a given slope. Values greater than unity indicate higher shear strength, while values lower than one point to a very unstable slope. The factor of safety is a function of cohesion, moisture content, pore-pressure, internal friction angle, and slope angle. Figure 3(d) shows a comparison of both numerical and experimental trend of a slope under gradual wetting conditions. In the figure, an increase in moisture content which fuels an increase in negative pore-pressures together with a notable drop in cohesion will serve to lower the factor of safety to below unity, a state that exacerbates the slope to imminent failure. The factor of safety is observed to drop below unity when the pore-pressure rises to the positive phase. As alluded to earlier, pore-pressures may still rise even after a rainfall event, as in our experiment. Correspondingly, the factor of safety may also drop to below unity even after the rainfall event. In this case, the factor of safety dropped to below unity after approximately 50 min of the experiment. This explains why most slopes collapse some time after a rainfall event and not during the storm. Model and experimental results are in agreement except for a negligible number of experimental deviations with RMSE of 0.0385 and  $r^2$  of 0.6381.

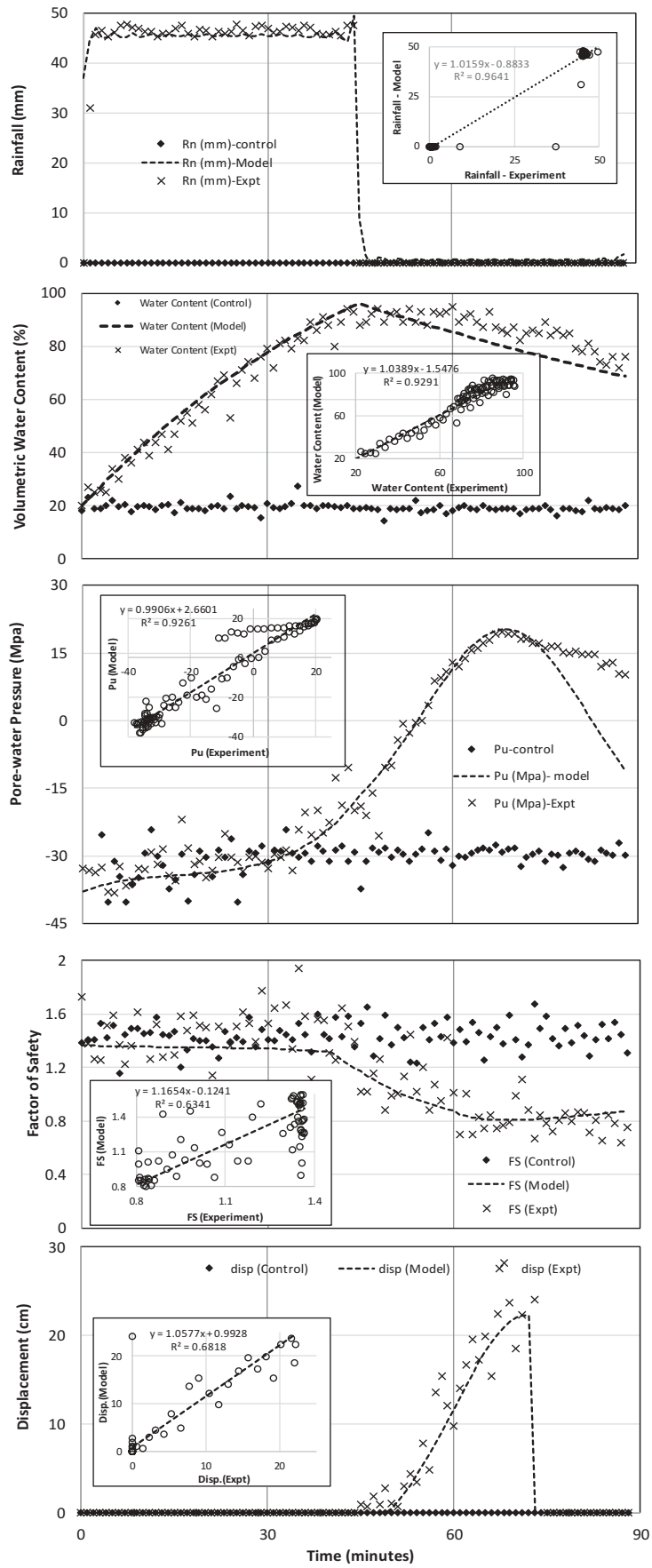


Figure 3. Computational and experimental results of (a) rainfall intensity; (b) water content; (c) pore-pressure; (d) factor of safety, and (e) displacement, as a function of time in minutes. Inset: statistical analysis.

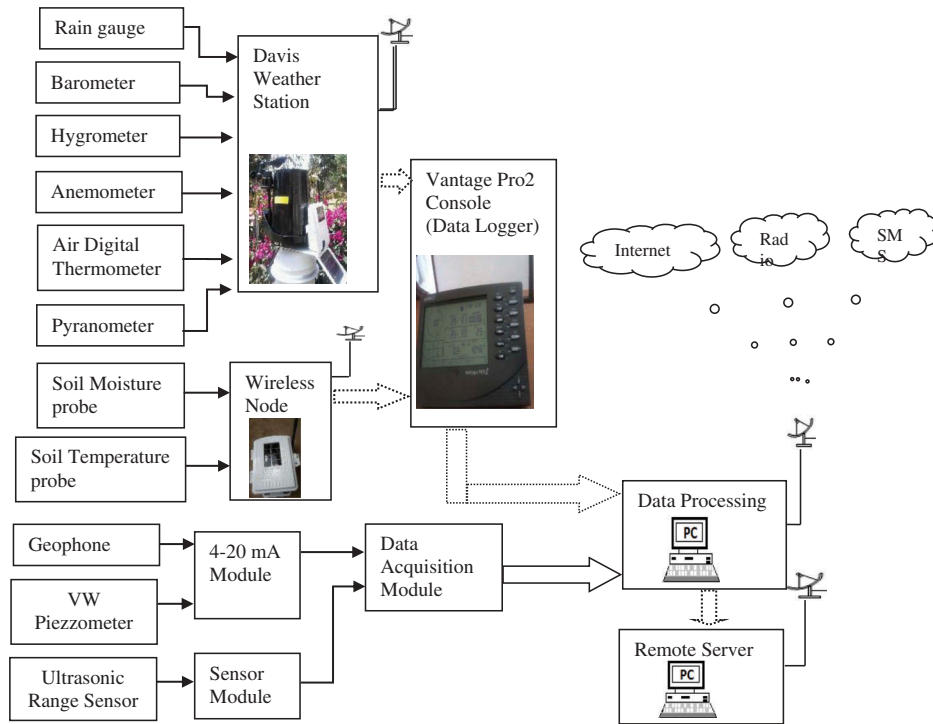


Figure 4. SPM flowchart.

The variation of factor of safety over time dictates the dynamics of a given slope. According to the Mohr–Coulomb failure criterion, the probability of translational failure is very high for any slope with values of factor of safety less than unity. Slope failure can be translational or circular. For relatively steep slopes, translational displacement is more probable as observed from these experiments. Because of erosion occurrences, especially for bare land, the resulting slope shape usually appears like a spherical cap with its diameter lying along the incline plane. When infiltration proceeds in this spherical-cap-shaped slope, part of the water increases its weight, while the other part creates a weak section along the incline plane through lubrication for nearly saturated conditions. Under these conditions, the cohesive strength of the soil mass will be lost, and the downward gravitational forces will exceed frictional forces leading to downward displacement. In the process, the soil mass will either be displaced as a whole but eventually break into smaller lumps or undergo liquefaction and flow as a liquid down the plane, depending on the type of being tested. For our case, the soil mass was undergoing liquefaction for all cases tested. Figure 3(e) illustrates the displacement characteristics of the soil mass over time with a comparison of the numerical model and experimental results. Again, model results marry well with the experimental findings depicting the accuracy of the model, i.e., RMSE as 0.1496 and  $r^2$  of 0.8257.

## 5 Conclusion and recommendations

The proposed numerical models regarding translational failure for a spherical-cap-shaped slope section have been shown to agree well with the experimental results obtained from measurements using the SPM system, specifically for shallow soil masses at steep slopes. The proposed model for the factor of safety and by extension the other hydrological models derived are unique in that they take into consideration the moist soil unit weight as opposed to earlier models which were applied only in extreme conditions of purely dry soil or saturated conditions. The model is also more convenient as it contains fewer variables as many of them are computed as empirical functions of water content. This model of factor of safety is convenient for shallow landslides at relatively steep slopes.

Since the study was confined to one particular angle throughout the experiment, we, therefore, recommend further investigations on the accuracy and reliability of this model at different angles. Similarly, different soil types should be tested to ascertain the reliability of these models. We also recommend an experimental testing of this model in the *in-situ* conditions at different locations.

## Acknowledgments

We acknowledge the support of Physics Department, Soil Science Department, University of Eldoret, and National Council for Science and Technology (NCST).



## Disclosure statement

No potential conflict of interest was reported by the authors.

## ORCID

J. Kanule  <http://orcid.org/0000-0003-3424-6204>

W. Ng'etich  <http://orcid.org/0000-0002-2650-3648>

## References

- Anderson, R. S., & Anderson, S. P. (2010). *Geomorphology: The mechanics and chemistry of landscapes* (pp. 637). Cambridge: Cambridge University Press.
- Bishop, A. W. (1967). Progressive failure—With special reference to the mechanism causing it. Panel Discussion. Proc. Geotech. Conf., Oslo 2, 142–150.
- De Vleeschauwer, C., & De Smedt, F. (2002). Modeling slope stability using GIS on a regional scale, *Proceedings of the first Geological Belgica International Meeting*, Leuven, 11–15 September 2002; *Aardkundige Mededelingen* 12, 253–256.
- Fang, H., Cui, P., Pei, L. Z., & Zhou, X. J. (2012). Model testing on rainfall-induced landslide of loose soil in Wenchuan earthquake region. *Natural Hazard and Earth System Sciences*, 12, 527–533.
- Guzzetti, F., Ardizzone, F., Cardinali, M., Rossi, M., & Valigi, D. (2009). Landslide volumes and landslide mobilization rates in Umbria, central Italy. *Earth and Planetary Science Letters*, 279(3–4), 222–229.
- Jia, G. W., Zhan, T. L. T., Chen, Y. M., & Fredlund, D. G. (2009). Performance of a largescale slope model subjected to rising and lowering water levels. *Engineering Geology*, 106(1–2), 92–103.
- Kilburn, C. R. J., & Petley, D. N. (2003). Forecasting giant, catastrophic slope collapse: Lessons from Vajont, Northern Italy. *Geomorphology*, 54(1–2), 21–32.
- Meunier, P., Hovius, N., & Haines, J. (2008). Topographic site effects and the location of earthquake induced landslides. *Elsevier: Earth and Planetary Science Letters*, 275, 221–232.
- Nahm, F. S. (2016). Nonparametric statistical tests for the continuous data: The basic concept and the practical use. *Korean Journal of Anesthesiology*, 69, 8–14.
- Najjar, Y. M., Ali, H. E., & Basheer, I. A. (1999). “On the use of neurons for simulating the stress-strain behavior of soils.” *Proc., 7th Int. Symposium on Numerical Models in Geomechanics*, eds. G. N. Pande, A. Graz, Graz, Austria, NUMOG VII, September 1–3, 657–662.
- Petley, D. (2009). Mass Movement Hazards. In K. Smith & D. Petley (Eds.), *Environmental Hazards: Assessing risk and reducing disaster* (pp. 416). London: Routledge.
- Ray, R. L., Jacobs, J. M., & de Alba, P. (2010). Impacts of unsaturated zone soil moisture and groundwater table on slope instability. *Journal of Geotechnical and Geoenvironmental Engineering*, 136(10), 1448–1458.
- Rybar, J., Stemberk, J., & Wagner, P. (2002). *Landslides: proceedings of the First European Conference on Landslides*, Prague, Czech Republic, June 24 201026. Taylor & Francis, Prague.
- Shahin, M. A., Jaksa, M. B., & Maier, H. R. (2001). Artificial neural network applications in geotechnical engineering. *Australian Geomechanics*, 36(1), 49–62.
- Sidle, R. C., & Ochiai, H. (2006). “*Landslides: Processes, prediction, and land use.*” *Water resources monograph*, Vol. 18. Washington, D.C: American Geophysical Union.
- van Genuchten, M., Th. (1980). A closed-form equation for predicting the hydraulic conductivity of unsaturated soils. *Soil Science Society of America Journal*, 44(5), 892–898.